A&A 496, 275–279 (2009)
DOI: 10.1051/0004-6361/200811235

Astronomy & Astrophysics

Accurate rest frequencies for the submillimetre-wave lines of the ^{15}N-containing isotopologues of N_2H^+ and N_2D^+

L. Dore, L. Bizzocchi, C. Degli Esposti, and F. Tinti

Dipartimento di Chimica "G. Ciamician", via F. Selmi 2, 40126 Bologna, Italy
e-mail: [luca.dore;luca.bizzocchi;claudio.degliesposti;francesca.tinti4]@unibo.it

Received 27 October 2008 / Accepted 13 January 2009

ABSTRACT

The submillimetre-wave spectrum of the molecular ions $N^{15}NH^+$, $^{15}NNH^+$, $N^{15}ND^+$, and $^{15}NND^+$ have been investigated in the laboratory using a source-modulation microwave spectrometer equipped with a negative glow discharge cell. The diazenylium ion was produced in a $Ar/N_2/H_2(D_2)$ discharge plasma and the ^{15}N-containing isotopologues were observed in natural abundance. Six new rotational transitions for the protonated species and seven for the deuterated ones were accurately measured in the frequency range 270–760 GHz. These new laboratory measurements of the rare isotopologues of N_2H^+ provide very precise rest frequencies at millimetre and submillimetre wavelengths useful for the radioastronomical identification of their rotational lines in the ISM.

Key words. molecular data – methods: laboratory – techniques: spectroscopic – radio lines: ISM

1. Introduction

Samples of primitive solar system materials, such as meteorites that reached the Earth's surface and the interplanetary dust particles (IDPs) returned by the *Stardust* mission, have shown anomalies and enhancements in various elemental isotopic ratios (e.g. Ehrenfreund & Charnley 2000; Clayton & Nittler 2004; McKeegan et al. 2006). In particular, the laboratory analyses have provided evidences of large D/H and $^{15}N/^{14}N$ ratios, which have been attributed to the survival of D- and ^{15}N-enriched material from the interstellar medium (ISM; Messenger 2000; Maret et al. 2006).

It has long been established that low-temperature gas-phase ion-molecule reactions and catalysis on the surface of cold interstellar dust grains lead to large D fractionation. In contrast, for nitrogen the situation is less clear due the scarcity of observational data and also because models of the ^{15}N fractionation in typical dense clouds predict only modest enhancements (Terzieva & Herbst 2000). Charnley & Rodgers (2002) has suggested that a significant increase of the ^{15}N-fractionation can occur if CO is depleted onto dust grains; the key fractionation process involves diazenylium ion via the exotermic reactions:

$$^{15}N + {}^{14}N_2H^+ \rightleftharpoons {}^{14}N + {}^{15}N^{14}NH^+, \quad (1a)$$

$$^{15}N + {}^{14}N_2H^+ \rightleftharpoons {}^{14}N + {}^{14}N^{15}NH^+, \quad (1b)$$

which preferentially drive ^{15}N into molecular nitrogen through the main dissociative recombination channel $N_2H^+ + e^- \rightarrow N_2 + H$ (Molek et al. 2007) at the expense of atomic N^0 which becomes isotopically light. Under normal interstellar conditions the degree of fractionation is limited by chemical reactions which exchange ^{14}N and ^{15}N between atomic and molecular forms:

$$N_2 \xrightarrow{He^+} N^0 \xrightarrow{OH} NO \xrightarrow{N^0} N_2. \quad (2)$$

However, if CO is frozen out, OH is unavailable, the cycle (2) is broken, and the processes (1) produce a larger ^{15}N-enhancement, which might explain the high $^{15}N/^{14}N$ ratio of the IDPs and meteoritic data (Rodgers & Charnley 2008). This picture, also predicts enhanced abundances of ^{15}N-bearing diazenylium in CO-depleted cores, thus the observation of N_2H^+, $N^{15}NH^+$, and $^{15}NNH^+$, and the determination of their isotopic ratio provides a very effective test for the reliability of the model (Charnley & Rodgers 2002)

Previous searches of $N^{15}NH^+$ and $^{15}NNH^+$ have been carried out long time ago (Womack et al. 1992; Linke et al. 1983) and the detection has been successful only toward massive star forming region, owing to the low sensitivity achieved and also because of the selection of sources, which did not focuse on cold, centrally concentrated cores showing heavy CO depletion, which were not known at that time. In CO-depleted regions, also deuterium fractionation increases, therefore N_2D^+ can be easily detected (see Dore et al. 2004), however its ^{15}N-containing isotopologues have not been observed until now, owing also to the lack of any accurate spectral data.

As for the laboratory spectroscopy of $N^{15}NH^+$ and $^{15}NNH^+$ is concerned, Gudeman (1982) reported the $J = 1 \leftarrow 0$ transitions; the spectrum of the former species was split into three components due to the quadrupole coupling of the external ^{14}N nucleus, while for the other species no hyperfine structure could be resolved. The only other transition detected in laboratory was the $J = 7 \leftarrow 6$ (Havenith et al. 1990), but with a ~1 MHz accuracy. No spectra, instead, are reported for the deuterated species $N^{15}ND^+$ and $^{15}NND^+$.

In order to provide reliable spectroscopic information for these species, we measured, in the region 270–760 GHz, transitions from $J = 3 \leftarrow 2$ to $J = 8 \leftarrow 7$ of $N^{15}NH^+$ and $^{15}NNH^+$, and from $J = 4 \leftarrow 3$ to $J = 10 \leftarrow 9$ of $N^{15}ND^+$ and $^{15}NND^+$. The newly obtained laboratory data, together with the previously determined ^{14}N-hyperfine constants (Caselli et al. 1995; Dore et al. 2004) allowed for the calculation of very accurate rest frequencies for all four ^{15}N-containing variants of N_2H^+ and N_2D^+ at millimetre and submillimetre wavelengths, the predicted uncertainties being less that 0.005 km s^{-1} up to 1 THz.

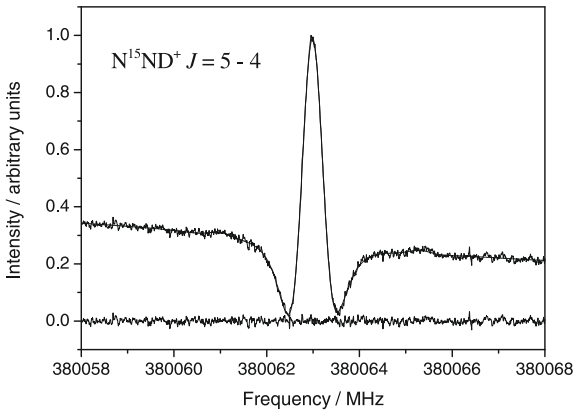

Fig. 1. Spectrum of the $J = 5-4$ rotational transition of $N^{15}ND^+$; total integration time 99 s at 1.6 MHz/s with time constant of 10 ms. The spectral profile has been fit to a sum of five hyperfine components; fit residuals are shown at the bottom of the plot.

Table 1. Rotational transition frequencies and spectroscopic constants of $N^{15}NH^+$.

J'	J	Observed (MHz)	Obs.-calc. (kHz)	Uncert.[a] (kHz)
1	0	91 205.7380[b]	43.5	50
3	2	273 608.9846	–2.9	5
4	3	364 802.5417	3.8	5
5	4	455 987.9927	0.6	5
6	5	547 163.3276	1.4	5
7	6	638 326.5101	–6.0	5
8	7	729 475.5408	3.0	5
rms_{res}[c] = 16.7 kHz				
σ[d] = 0.846				
Constant[e]			Correlation matrix	
B_0 / MHz	45 603.01594(41)	1.000		
D_J / kHz	84.3346(42)	–0.928	1.000	

[a] Uncertainties estimated as explained in the text.
[b] From Gudeman (1982).
[c] Rms error of residuals: $\sqrt{\frac{\sum \text{residual}^2}{N \text{ observations}}}$.
[d] Fit standard deviation: $\sqrt{\frac{\sum (\text{residual/uncert.})^2}{\text{degrees of freedom}}}$.
[e] Standard errors are reported in parentheses in units of the last quoted digits.

2. Experimental details and data analysis

The rotational spectra of the four isotopologues of N_2H^+ and N_2D^+ containing ^{15}N were observed with a frequency-modulated millimetre-wave spectrometer (Cazzoli & Dore 1990) equipped with a negative glow discharge cell made of a Pyrex tube, 3.25 m long and 5 cm in diameter, with two cylindrical hollow electrodes 25 cm in length at either end. The radiation source was a frequency multiplier, built by a doubler in cascade with a multiplier (RPG – Radiometer Physics GmbH), which was driven by Gunn oscillators working in the region 67–105 GHz (Farran Technology Limited, RPG – Radiometer Physics GmbH). Two phase-lock loops allow the stabilisation of the Gunn oscillator with respect to a frequency synthesizer, which is driven by a 5-MHz rubidium frequency standard. The frequency modulation of the radiation is obtained by sine-wave modulating at 16.66 kHz the reference signal of the wide-band Gunn-synchronizer (total harmonic distortion less than 0.01%). The signal, detected by a liquid-helium-cooled InSb hot electron bolometer (QMC Instr. Ltd. type QFI/2), is demodulated at $2f$ by a lock-in amplifier.

N_2H^+ (or N_2D^+) was produced in a DC discharge by flowing a 1:1 mixture of N_2 and H_2 (D_2) (3 mTorr, 0.4 Pa) with addition of Ar buffer gas for a total pressure of about 10 mTorr (1.3 Pa). The ^{15}N-containing species were observed in natural abundance. The discharge current was a few mA, the Pyrex cell was cooled at about 80 K by liquid nitrogen circulation in an external plastic pipe tightly wound around it, and an axial magnetic field up to about 110 G was applied throughout the length of the discharge. It is well established (see Tinti et al. 2007) that, with this magnetic confinement, the ions are produced and observed in a nearly field free region, the negative glow, thus they do not show any Doppler shift due to the drift velocity.

Table 2. Rotational transition frequencies and spectroscopic constants of $^{15}NNH^+$.

J'	J	Observed (MHz)	Obs.-calc. (kHz)	Uncert.[a] (kHz)
1	0	90 263.8330[b]	–2.3	10.
3	2	270 783.5870	8.1	20.
4	3	361 035.5242	0.7	5.
5	4	451 279.5385	–2.4	5.
6	5	541 513.6509	1.5	5.
7	6	631 735.8673	0.2	5.
8	7	721 944.2091	–3.1	15.
rms_{res}[c] = 3.6 kHz				
σ[d] = 0.350				
Constant[e]			Correlation matrix	
B_0 / MHz	45 132.08283(23)	1.000		
D_J / kHz	82.5747(28)	–0.943	1.000	

[a] Uncertainties estimated as explained in the text.
[b] From Gudeman (1982).
[c] Rms error of residuals: $\sqrt{\frac{\sum \text{residual}^2}{N \text{ observations}}}$.
[d] Fit standard deviation: $\sqrt{\frac{\sum (\text{residual/uncert.})^2}{\text{degrees of freedom}}}$.
[e] Standard errors are reported in parentheses in units of the last quoted digits.

Table 3. Rotational transition frequencies and spectroscopic constants of $N^{15}ND^+$.

J'	J	Observed (MHz)	Obs.-calc. (kHz)	Uncert.[a] (kHz)
4	3	304 058.9449	–0.8	5.
5	4	380 062.9822	0.3	5.
6	5	456 059.8857	1.1	5.
7	6	532 048.2255	–1.7	5.
8	7	608 026.5845	1.6	5.
9	8	683 993.5241	–0.9	5.
10	9	759 947.6328	5.9	30.
rms_{res}[b] = 2.5 kHz				
σ[c] = 0.270				
Constant[d]			Correlation matrix	
B_0 / MHz	38 009.27047(12)	1.000		
D_J / kHz	59.44560(95)	–0.935	1.000	

[a] Uncertainties estimated as explained in the text.
[b] Rms error of residuals: $\sqrt{\frac{\sum \text{residual}^2}{N \text{ observations}}}$.
[c] Fit standard deviation: $\sqrt{\frac{\sum (\text{residual/uncert.})^2}{\text{degrees of freedom}}}$.
[d] Standard errors are reported in parentheses in units of the last quoted digits.

Table 4. Rotational transition frequencies and spectroscopic constants of $^{15}NND^+$.

J'	J	Observed (MHz)	Obs.-calc. (kHz)	Uncert.[a] (kHz)
4	3	299 029.7997	4.9	5.
5	4	373 776.8770	2.4	5.
6	5	448 517.0446	2.7	5.
7	6	523 248.9086	–5.5	5.
8	7	597 971.1055	–3.2	5.
9	8	672 682.2388	–4.4	5.
10	9	747 380.9405	5.5	5.

rms_{res} [b] = 4.2 kHz
σ^c = 1.006

Constant[d]		Correlation matrix	
B_0 / MHz	37 380.56770(36)	1.000	
D_J / kHz	57.6047(25)	–0.932	1.000

[a] Uncertainties estimated as explained in the text.

[b] Rms error of residuals: $\sqrt{\frac{\sum \text{residual}^2}{N \text{ observations}}}$.

[c] Fit standard deviation: $\sqrt{\frac{\sum (\text{residual/uncert.})^2}{\text{degrees of freedom}}}$.

[d] Standard errors are reported in parentheses in units of the last quoted digits.

Table 5. Predicted rest-frequencies, estimated 1σ uncertainties, and line strengths for $N^{15}NH^+$.

J'	F'	J	F	Rest frequency (MHz)	Uncertainty (kHz)	Line strength
1	1	0	1	91 204.2602	0.0009	1.000
1	2	0	1	91 205.9908	0.0008	1.667
1	0	0	1	91 208.5162	0.0012	0.333
2	2	1	2	182 407.6345	0.0017	0.500
2	1	1	0	182 407.9308	0.0016	0.667
2	2	1	1	182 409.3651	0.0015	1.500
2	3	1	2	182 409.4987	0.0015	2.800
2	1	1	1	182 412.1867	0.0017	0.500
3	2	2	1	273 608.6912	0.0020	1.800
3	3	2	2	273 608.9875	0.0020	2.667
3	4	2	3	273 609.0670	0.0020	3.857
4	3	3	2	364 802.4042	0.0023	2.857
4	4	3	3	364 802.5379	0.0023	3.750
4	5	3	4	364 802.5927	0.0023	4.889
5	4	4	3	455 987.9126	0.0022	3.889
5	5	4	4	455 987.9921	0.0022	4.800
5	6	4	5	455 988.0337	0.0022	5.909
6	5	5	4	547 163.2713	0.0020	4.909
6	6	5	5	547 163.3262	0.0020	5.833
6	7	5	6	547 163.3598	0.0020	6.923
7	6	6	5	638 326.4745	0.0022	5.923
7	7	6	6	638 326.5161	0.0022	6.857
7	8	6	7	638 326.5446	0.0022	7.933
8	7	7	6	729 475.5042	0.0036	6.933
8	8	7	7	729 475.5378	0.0036	7.875
8	9	7	8	729 475.5628	0.0036	8.941
9	8	8	7	820 608.3388	0.0063	7.941
9	9	8	8	820 608.3673	0.0063	8.889
9	10	8	9	820 608.3897	0.0063	9.947
10	9	9	8	911 722.9555	0.0100	8.947
10	10	9	9	911 722.9805	0.0100	9.900
10	11	9	10	911 723.0011	0.0100	10.952
11	10	10	9	1 002 817.3309	0.0148	9.952
11	11	10	10	1 002 817.3534	0.0148	10.909
11	12	10	11	1 002 817.3726	0.0148	11.957

Table 6. Predicted rest-frequencies, estimated 1σ uncertainties, and line strengths for $^{15}NNH^+$.

J'	F'	J	F	Rest frequency (MHz)	Uncertainty (kHz)	Line strength
1	1	0	1	90 263.4870	0.0009	1.000
1	2	0	1	90 263.9120	0.0006	1.667
1	0	0	1	90 264.4972	0.0016	0.333
2	2	1	2	180 525.2639	0.0014	0.500
2	1	1	0	180 525.3405	0.0011	0.667
2	2	1	1	180 525.6889	0.0008	1.500
2	3	1	2	180 525.7267	0.0009	2.800
2	1	1	1	180 526.3508	0.0018	0.500
3	2	2	1	270 783.5022	0.0012	1.800
3	3	2	2	270 783.5789	0.0011	2.667
3	4	2	3	270 783.6038	0.0012	3.857
4	3	3	2	361 035.4857	0.0012	2.857
4	4	3	3	361 035.5235	0.0012	3.750
4	5	3	4	361 035.5425	0.0012	4.889
5	4	4	3	451 279.5160	0.0011	3.889
5	5	4	4	451 279.5409	0.0010	4.800
5	6	4	5	451 279.5567	0.0011	5.909
6	5	5	4	541 513.6303	0.0010	4.909
6	6	5	5	541 513.6494	0.0009	5.833
6	7	5	6	541 513.6633	0.0010	6.923
7	6	6	5	631 735.8512	0.0015	5.923
7	7	6	6	631 735.8671	0.0014	6.857
7	8	6	7	631 735.8798	0.0015	7.933
8	7	7	6	721 944.1983	0.0027	6.933
8	8	7	7	721 944.2122	0.0027	7.875
8	9	7	8	721 944.2241	0.0027	8.941
9	8	8	7	812 136.6903	0.0047	7.941
9	9	8	8	812 136.7030	0.0046	8.889
9	10	8	9	812 136.7143	0.0047	9.947
10	9	9	8	902 311.3458	0.0073	8.947
10	10	9	9	902 311.3576	0.0073	9.900
10	11	9	10	902 311.3685	0.0073	10.952
11	10	10	9	992 466.1831	0.0106	9.952
11	11	10	10	992 466.1944	0.0106	10.909
11	12	10	11	992 466.2049	0.0106	11.957

The spectra were recorded by sweeping the frequency up and down (several times if signal averaging is needed) in steps of 5 or 10 kHz with an acquisition time of 8–18 ms per step: the lock-in amplifier time constant was set at 10 ms.

It has to be pointed out that low-J rotational lines of $^{14}N^{15}NH^+$ and $^{14}N^{15}ND^+$, with the quadrupolar ^{14}N nucleus in the external position, are split by hyperfine interactions; however, the transitions recorded in the present work appear as a main blended peak, produced by the collapsed $\Delta F = +1$ triplet, with two very weak $\Delta F = 0$ features at its both sides apparent only with a high signal to noise ratio. Therefore, the unperturbed line frequency was recovered by a line shape analysis of the spectral profile modeled as a sum of hyperfine components with their frequency shift and intensity fixed at the values accurately predicted using the hyperfine constants known from literature (Caselli et al. 1995; Dore et al. 2004). Figure 1 illustrates a recording of the $J = 5 \leftarrow 4$ transition of the $N^{15}ND^+$ isotopologue analyzed in this way. The same procedure, which also accounts for the frequency modulation and the line asymmetry due to etalon effects in the cell (see Dore 2003), was used to analyze the spectra of $^{15}N^{14}NH^+$ and $^{15}N^{14}ND^+$ as well.

Since each transition was recorded several times, its frequency was derived as the mean of the determined unperturbed line centers, with an uncertainty estimated from the root mean square error of their distribution. When such uncertainty resulted

Table 7. Predicted rest-frequencies, estimated 1σ uncertainties, and line strengths for $N^{15}ND^+$.

J'	F'	J	F	Rest frequency (MHz)	Uncertainty (kHz)	Line strength
1	1	0	1	76 016.8733	0.0010	1.000
1	2	0	1	76 018.5970	0.0006	1.667
1	0	0	1	76 021.1239	0.0019	0.333
2	2	1	2	152 033.4559	0.0015	0.500
2	1	1	0	152 033.7497	0.0010	0.667
2	2	1	1	152 035.1796	0.0004	1.500
2	3	1	2	152 035.3111	0.0007	2.800
2	1	1	1	152 038.0004	0.0019	0.500
3	2	2	1	228 048.9089	0.0008	1.800
3	3	2	2	228 049.2027	0.0006	2.667
3	4	2	3	228 049.2801	0.0008	3.857
4	3	3	2	304 058.8142	0.0009	2.857
4	4	3	3	304 058.9457	0.0007	3.750
4	5	3	4	304 058.9985	0.0009	4.889
5	4	4	3	380 062.9045	0.0009	3.889
5	5	4	4	380 062.9819	0.0007	4.800
5	6	4	5	380 063.0214	0.0009	5.909
6	5	5	4	456 059.8318	0.0009	4.909
6	6	5	5	456 059.8846	0.0007	5.833
6	7	5	6	456 059.9162	0.0009	6.923
7	6	6	5	532 048.1876	0.0008	5.923
7	7	6	6	532 048.2272	0.0006	6.857
7	8	6	7	532 048.2536	0.0008	7.933
8	7	7	6	608 026.5512	0.0009	6.933
8	8	7	7	608 026.5829	0.0007	7.875
8	9	7	8	608 026.6058	0.0009	8.941
9	8	8	7	683 993.4985	0.0012	7.941
9	9	8	8	683 993.5250	0.0011	8.889
9	10	8	9	683 993.5454	0.0012	9.947
10	9	9	8	759 947.6039	0.0019	8.947
10	10	9	9	759 947.6269	0.0018	9.900
10	11	9	10	759 947.6455	0.0019	10.952
11	10	10	9	835 887.4414	0.0029	9.952
11	11	10	10	835 887.4618	0.0028	10.909
11	12	10	11	835 887.4790	0.0029	11.957
12	11	11	10	911 811.5845	0.0041	10.957
12	12	11	11	911 811.6031	0.0041	11.917
12	13	11	12	911 811.6192	0.0041	12.960
13	12	12	11	987 718.6069	0.0057	11.960
13	13	12	12	987 718.6240	0.0057	12.923
13	14	12	13	987 718.6392	0.0057	13.963

Table 8. Predicted rest-frequencies, estimated 1σ uncertainties, and line strengths for $^{15}NND^+$.

J'	F'	J	F	Rest frequency (MHz)	Uncertainty (kHz)	Line strength
1	1	0	1	74 760.5619	0.0016	1.000
1	2	0	1	74 760.9788	0.0010	1.667
1	0	0	1	74 761.5650	0.0029	0.333
2	2	1	2	149 520.0106	0.0024	0.500
2	1	1	0	149 520.0844	0.0020	0.667
2	2	1	1	149 520.4274	0.0014	1.500
2	3	1	2	149 520.4628	0.0015	2.800
2	1	1	1	149 521.0874	0.0031	0.500
3	2	2	1	224 277.1110	0.0020	1.800
3	3	2	2	224 277.1849	0.0019	2.667
3	4	2	3	224 277.2074	0.0020	3.857
4	3	3	2	299 029.7594	0.0024	2.857
4	4	3	3	299 029.7948	0.0023	3.750
4	5	3	4	299 029.8115	0.0024	4.889
5	4	4	3	373 776.8521	0.0026	3.889
5	5	4	4	373 776.8746	0.0025	4.800
5	6	4	5	373 776.8882	0.0026	5.909
6	5	5	4	448 517.0252	0.0026	4.909
6	6	5	5	448 517.0419	0.0025	5.833
6	7	5	6	448 517.0536	0.0026	6.923
7	6	6	5	523 248.9005	0.0024	5.923
7	7	6	6	523 248.9141	0.0022	6.857
7	8	6	7	523 248.9245	0.0024	7.933
8	7	7	6	597 971.0970	0.0022	6.933
8	8	7	7	597 971.1087	0.0021	7.875
8	9	7	8	597 971.1183	0.0022	8.941
9	8	8	7	672 682.2327	0.0027	7.941
9	9	8	8	672 682.2432	0.0026	8.889
9	10	8	9	672 682.2522	0.0027	9.947
10	9	9	8	747 380.9254	0.0041	8.947
10	10	9	9	747 380.9350	0.0041	9.900
10	11	9	10	747 380.9436	0.0041	10.952
11	10	10	9	822 065.7927	0.0065	9.952
11	11	10	10	822 065.8018	0.0064	10.909
11	12	10	11	822 065.8100	0.0065	11.957
12	11	11	10	896 735.4523	0.0095	10.957
12	12	11	11	896 735.4609	0.0095	11.917
12	13	11	12	896 735.4689	0.0095	12.960
13	12	12	11	971 388.5215	0.0134	11.960
13	13	12	12	971 388.5298	0.0134	12.923
13	14	12	13	971 388.5376	0.0134	13.963

to be less than 5 kHz, it was given a 5 kHz value, to account for a possible tiny pressure shift, whose value and sign are difficult to estimate, which, for instance for HCO^+ broadened by Argon, has an absolute value less than 1 kHz/mTorr (Buffa et al. 2006).

The determined experimental transition frequencies were fitted, in a weighted-least-squares procedure, to the standard frequency expression of the rotational transition $J + 1 \leftarrow J$:

$$\nu_0 = 2B_0(J + 1) - 4D_J(J + 1)^3, \quad (3)$$

where B_0 and D_J are the ground-state rotational and quartic centrifugal distortion constants, respectively; the weights were the inverse-square of the uncertainties. The values of the spectroscopic constants of $N^{15}NH^+$, $^{15}NNH^+$, $N^{15}ND^+$, and $^{15}NND^+$ derived from the fits are reported in Tables 1–4.

3. Discussion

This paper reports new laboratory measurements of the the rotational spectra of ^{15}N-containing variants of diazenylium ion at millimetre and submillimetre wavelengths (270–760 GHz). Six and seven rotational transitions were accurately determined for the H- and D-containing pairs of isotopic species, respectively. Efforts were made in order to minimize the significance of the the most common sources of systematic error in the determination of the line positions. The precision of the data is also excellent: only in few instances the least-squares residuals exceed 5 kHz, which is a very low value for Doppler limited measurements.

The accuracy of the determined spectroscopic constants is even higher than that attained by Amano et al. (2005) in their paper concerning the main isotopologues $^{14}N_2H^+$ and $^{14}N_2D^+$. Thus, the present rotational, B_0, and quartic centrifugal distortion, D_J, constants allow the calculation of a very reliable set of rest frequencies for the four isotopologues $N^{15}NH^+$, $^{15}NNH^+$, $N^{15}ND^+$, and $^{15}NND^+$ at millimetre and submillimetre wavelengths. The predicted 1σ uncertainties at 1 THz are, even in the less favourable case, less than 0.01 km s^{-1}, whereas they are only

few thousandths of km s^{-1} for the 3 mm band $J = 1-0$ transition of all species.

Tables 5–8 collect a list of rest frequencies up to 1 THz calculated from the spectroscopic constants of Tables 1–4 and include also the estimated uncertainty at 1σ level obtained by propagation of the standard errors of spectroscopic and hyperfine constants. The hyperfine structure of each transition has been predicted, assuming the hyperfine constants of Caselli et al. (1995) and Dore et al. (2004), by means of the SPCAT prediction program (Pickett 1991), and the hyperfine components included in each multiplet collect at least the 90% of the total intensity of the relevant $J + 1 - J$ rotational transition. The line strength value, S_{ij}, is defined as the square of the reduced matrix element of the rotation matrix (Brown & Carrington 2003)

$$S_{ij} = \left|\langle J_i F_i \left\| \mathscr{D}^{(1)}_{\cdot q}(\omega)^* \right\| J_j F_j \rangle\right|^2 . \quad (4)$$

The intensity of a line in absorption can be obtained by multiplying the line strength S_{ij} by the square of the dipole moment μ, by the transition frequency and by the population factor of the lower level. The Einstein A-coefficients for spontaneous emission from state i to j can also be calculated from the line strengths by use of

$$A_{i\to j} = \frac{16\pi^3 \nu_{ij}^3}{3\epsilon_0 hc^3} \frac{1}{2F_i + 1} S_{ij}\mu^2. \quad (5)$$

Acknowledgements. This work has been supported by MIUR (PRIN 2007 funds, project "Trasferimenti di energia, carica e molecole in sistemi complessi") and by University of Bologna (RFO funds).

References

Amano, T., Hirao, T., & Takano, J. 2005, J. Mol. Spectrosc., 234, 170
Brown, J., & Carrington, A. 2003, Rotational Spectroscopy of Diatomic Molecules (Cambridge)
Buffa, G., Dore, L., Tinti, F., & Meuwly, M. 2006, Chem. Phys. Chem., 7, 1764
Caselli, P., Myers, P. C., & Thaddeus, P. 1995, ApJ, 455, L77
Cazzoli, G., & Dore, L. 1990, J. Mol. Spectrosc., 141, 49
Charnley, S. B., & Rodgers, S. D. 2002, ApJ, 569, L133
Clayton, D. D., & Nittler, L. R. 2004, ARA&A, 42, 39
Dore, L. 2003, J. Mol. Spectrosc., 221, 93
Dore, L., Caselli, P., Beninati, S., et al. 2004, A&A, 413, 1177
Ehrenfreund, P., & Charnley, S. B. 2000, ARA&A, 38, 427
Gudeman, C. S. 1982, Ph.D. Thesis, University of Winsconsin-Madison
Havenith, M., Zwart, E., Meerts, W. L., & ter Meulen, J. J. 1990, J. Chem. Phys., 93, 8446
Maret, S., Bergin, E. A., & Lada, C. J. 2006, Nature, 442, 425
McKeegan, K. D., Aléon, J., Bradley, J., et al. 2006, Science, 314, 1724
Messenger, S. 2000, Nature, 404, 968
Molek, C. D., McLain, J. L., Poterya, V., & Adams, N. G. 2007, J. Phys. Chem. A, 111, 6760
Pickett, H. M. 1991, J. Mol. Spectrosc., 148, 371
Rodgers, S. D., & Charnley, S. B. 2008, MNRAS, 385, L48
Terzieva, R., & Herbst, E. 2000, MNRAS, 317, 563
Tinti, F., Bizzocchi, L., Esposti, C. D., & Dore, L. 2007, ApJ, 669, L113